Dedicated Breast Computed Tomography With a Photon-Counting Detector: Initial Results of Clinical In Vivo Imaging

Berger, Nicole ; Marcon, Magda ; Saltybaeva, Natalia ; Kalender, Willi A ; Alkadhi, Hatem ; Frauenfelder, Thomas ; Boss, Andreas

Abstract: OBJECTIVES: The purpose of this work is to present the data obtained from the first clinical in vivo application of a new dedicated spiral breast computed tomography (B-CT) equipped with a photon-counting detector. MATERIALS AND METHODS: The institutional review board approved this retrospective study. Twelve women referred for breast cancer screening were included and underwent bilateral spiral B-CT acquired in prone position. Additional sonography was performed in case of dense breast tissue or any B-CT findings. In 3 women, previous mammography was available for comparison. Soft tissue (ST) and high-resolution (HR) images were reconstructed. Two independent radiologists performed separately the readout for subjective image quality and for imaging findings detection. Objective image quality evaluation was performed in consensus and included spatial resolution, contrast resolution, signal-to-noise ratio (SNR), and contrast-to-noise ratio. All women were asked to report about positioning comfort and overall comfort during data acquisition. RESULTS: The major pectoral muscle was included in 15 breast CT scans (62.5%); glandular component was partially missing in 2 (8.3%) of the 24 scanned breasts. A thin "ring artifact" was present in all scans but had no influence on image interpretations; no other artifacts were present. Subjective image quality assessment showed excellent agreement between the 2 readers ($\kappa = 1$). Three masses were depicted in B-CT and were confirmed as simple cysts in sonography. Additional 5 simple cysts and 2 solid benign lesions were identified only in sonography. A total of 12 calcifications were depicted with a median size of 1.1 mm (interquartile range, 0.7-1.7 mm) on HR and 1.4 mm (interquartile range, 1.1-1.8 mm) on ST images. Median SNRgl, SNRfat, and contrast-to-noise ratio were significantly higher in ST than in HR reconstructions (each, $P < 0.001$). A mild discomfort due to positioning of the rib cage on the table was reported by 2 women (16.7%); otherwise, no discomfort was reported. CONCLUSIONS: The new dedicated B-CT equipped with a photon-counting detector provides high-quality images with potential for screening of breast cancer along with minor patient discomfort.

DOI: https://doi.org/10.1097/RLI.0000000000000552

Dedicated Breast Computed Tomography With a Photon-Counting Detector

Initial Results of Clinical In Vivo Imaging

Nicole Berger, MD, Magda Marcon, MD,* Natalia Saltybaeva, PhD,* Willi A. Kalender, PhD,† Hatem Alkadhi, MD, MPH, EBCR,* Thomas Frauenfelder, MD,* and Andreas Boss, MD, PhD**

Objectives: The purpose of this work is to present the data obtained from the first clinical in vivo application of a new dedicated spiral breast computed tomography (B-CT) equipped with a photon-counting detector.

Materials and Methods: The institutional review board approved this retrospective study. Twelve women referred for breast cancer screening were included and underwent bilateral spiral B-CT acquired in prone position. Additional sonography was performed in case of dense breast tissue or any B-CT findings. In 3 women, previous mammography was available for comparison. Soft tissue (ST) and high-resolution (HR) images were reconstructed. Two independent radiologists performed separately the readout for subjective image quality and for imaging findings detection. Objective image quality evaluation was performed in consensus and included spatial resolution, contrast resolution, signal-to-noise ratio (SNR), and contrast-to-noise ratio. All women were asked to report about positioning comfort and overall comfort during data acquisition.

Results: The major pectoral muscle was included in 15 breast CT scans (62.5%); glandular component was partially missing in 2 (8.3%) of the 24 scanned breasts. A thin "ring artifact" was present in all scans but had no influence on image interpretations; no other artifacts were present. Subjective image quality assessment showed excellent agreement between the 2 readers ($\kappa = 1$). Three masses were depicted in B-CT and were confirmed as simple cysts in sonography. Additional 5 simple cysts and 2 solid benign lesions were identified only in sonography. A total of 12 calcifications were depicted with a median size of 1.1 mm (interquartile range, 0.7–1.7 mm) on HR and 1.4 mm (interquartile range, 1.1–1.8 mm) on ST images. Median SNR_{gl}, SNR_{fat}, and contrast-to-noise ratio were significantly higher in ST than in HR reconstructions (each, $P < 0.001$). A mild discomfort due to positioning of the rib cage on the table was reported by 2 women (16.7%); otherwise, no discomfort was reported.

Conclusions: The new dedicated B-CT equipped with a photon-counting detector provides high-quality images with potential for screening of breast cancer along with minor patient discomfort.

Key Words: breast CT, mammography, breast cancer screening

(*Invest Radiol* 2019;00: 00–00)

Two-view mammography is the standard imaging modality used for screening and diagnosis of breast cancer, representing the only modality with proven benefits in terms of lower mortality.[1–3] The main issue of mammography is its projection-based technique, which results in overlap of imaged structures with possible obscuration of suspicious lesions, especially in women with dense breast.[4] To ameliorate this limitation, digital breast tomosynthesis has been introduced in the recent years, showing improvements in terms of breast cancer detection.[5–9] Compared with the single projection image of mammography, in digital breast tomosynthesis, multiple low-dose projections are acquired from different angles and subsequently used to produce stacks of image slices, which can in part reduce the mammography overlapping effect, however, with rather low resolution in the z-direction.[10]

Dedicated breast computed tomography (B-CT) systems have been recently introduced, which can provide cross-sectional images with high isotropic spatial resolution and better soft tissue (ST) contrast. Breast computed tomography has the potential to further improve breast lesion detection and characterization compared with mammography and tomosynthesis.[11–13] Previous studies investigating the use of cone beam B-CT in comparison to mammography reported higher radiation doses for B-CT, especially when referring to a screening setting.[13,14] More recently, new strategies have strongly increased the dose efficiency due to the use of novel photon-counting detector technology, resulting in dose levels for B-CT comparable to those of screening mammography or lower.[15,16] In conventional energy-integrating detectors (EIDs), the electrical signal is generated by a photodiode, which detects the visible light produced by the interaction of the x-ray photons with a scintillator material. Photo-counting detectors count individual photons, and each count is allocated in specific energy bins related to the photon energy, providing direct conversion of x-ray photon energy into electric charge.[17] Due to this direct conversion, photo-counting detectors offer higher dose efficiency at smaller detector pixel size compared with conventional EID.[16,18]

Additional considerations relate to the fact that both mammography and tomosynthesis require breast compression to increase tissue contrast and to reduce radiation dose. This can be barely tolerated by some women or even represents the main reason for abstaining from mammographic examination.[19] In B-CT, no compression is required, thus meeting the needs also of those women. Lastly, the possibility to perform contrast-enhanced examinations indicates a possible usage of B-CT comparable to breast magnetic resonance (MR) imaging with the additional capability to simultaneously detect microcalcifications and ST contrast enhancement.

The purpose of this study was to present the results of first clinical in vivo applications of a new dedicated spiral B-CT equipped with a photon-counting detector.

MATERIALS AND METHODS

Patient Population

This retrospective study was approved by the local ethics committee "Kantonale Ethikkommission Zürich" (approval number: 2016-00064). All women included in the study provided written consent to a general informed consent for data treatment at the University Hospital Zürich.

Received for publication December 3, 2018; and accepted for publication, after revision, January 2, 2019.

From the *Institute of Diagnostic and Interventional Radiology, University Hospital Zurich, University of Zurich, Zurich, Switzerland; and †Institute of Medical Physics, University of Erlangen-Nürnberg, Germany.

Nicole Berger and Magda Marcon both contributed equally to this study.

Conflict of interest and sources of funding: This work was supported by a "Promedica-Stiftung" grant to M. Marcon and by a "Filling the Gap" grant to N. Berger. The funding sources were not involved in study design; in collection; analysis and interpretation of data; in manuscript writing; or in the decision to submit the manuscript for publication.

Correspondence to: Magda Marcon, MD, Institute of Diagnostic and Interventional Radiology, University Hospital Zurich, Ramistrasse 100, 8091 Zürich, Switzerland. E-mail: magda.marcon@usz.ch.

ISSN: 0020-9996/19/0000–0000
DOI: 10.1097/RLI.0000000000000552

Breast computed tomography examination was offered as an alternative to mammography to women undergoing opportunistic screening who would have not otherwise performed the mammography because of the pain due to the compression of the breasts. Women were admitted to undergo B-CT examination only if they were older than 40 years and had no mammographic examinations performed less than 12 months prior. We included consecutive examinations performed in August 2018. Estimation of breast density on B-CT images as well as image evaluation for lesion detection was initially performed in consensus by 2 radiologists immediately after the B-CT data acquisition and image reconstruction based on assumptions commonly applied to mammography according to the American College of Radiology (ACR) Breast Imaging Reporting and Data System (BI-RADS), fifth edition.[20] Included women with dense breast or any finding in B-CT images additionally underwent sonography, either using hand-held ultrasound or applying an automated breast ultrasound system (ABUS). In all women with previous mammography examinations, B-CT images were compared with previous mammograms. In all cases undergoing additional sonography, findings were noted and compared with previous sonographic examinations when available.

Technical support of the vendor was available; however, the evaluation of patient data and the integrity of the study were completely under the control of the first and last authors.

Dedicated Breast CT System

Examinations were performed placing the woman in a prone position on a dedicated spiral B-CT system (nu:view; AB-CT [Advanced Breast CT] GmbH, Erlangen, Germany). The examination table has a horizontal CT gantry optimized for breast imaging, which allows the examination of one breast at a time while the other breast and the rest of the body are not exposed. The examined breast was positioned in a table aperture without compression (Fig. 1). The ipsilateral arm was placed alongside the body, and the contralateral arm was elevated above the head. All participants were instructed to breath regularly during the scanning to minimize the possibility of movement artifacts.

The photon-counting detector uses cadmium telluride crystals with a detector pixel size of $(0.1\ mm)^2$ and a total detector area of $280 \times 50\ mm^2$. The maximum possible volume to examine has a diameter of 190 mm; the scanned length can be chosen at 3 different levels (80, 120, and 160 mm) depending on the anteroposterior breast diameter.

FIGURE 1. The examination table has a horizontal CT gantry, and the examined breast is placed in a table aperture in a plastic cylinder without compression. The maximum possible breast volume to examine has a diameter of 190 mm and a height of 160 mm. Scan length can be adjusted at 3 different levels (80, 120, and 160 mm) depending on the anteroposterior breast diameter.

TABLE 1. B-CT Parameters

X-ray tube current	5–125 mA "HighRes"; 5–64 mA "Standard"
X-ray tube voltage	60 kV
Data acquisition rate	Up to 1000 Hz
No. projections	Up to 2000 per 360 degrees
No. reconstruction images*	ST, 313–589; HR, 626–1178
Reconstruction field of measurement	200 × 80–160 mm
Acquisition time*	7–12 s/scan

*Depending on the scan length.

ST indicates soft tissue reconstruction; HR, high-resolution reconstruction.

Depending on the specified scan length, the x-ray tube loading time is automatically adjusted. The x-ray tube has a 0.3-mm focal spot size and 3-mm Al filtration. A fixed x-ray tube voltage of 60 kV is used to achieve sufficient contrast for visualization of microcalcifications. Data acquisition can be performed by choosing between 2 modes: in the first so-called "HighRes" acquisition mode, the entire breast volume can be scanned up to 2 times within a predetermined time and the highest possible spatial resolution is achieved; in the second so-called "standard" acquisition mode, the entire breast volume can be scanned up to 4 consecutive times allowing for dynamic measurements over the time (eg, after contrast agent injection). In the "standard" acquisition mode, the number of projections is inferior compared with "HighRes," and this makes possible the acquisition of consecutive image datasets without interruption necessary for data transmission. The tube current can be varied between 5 and 125 mA. Additional parameters are reported in Table 1. All examinations were performed using the "HighRes" acquisition mode considering the screening purpose of the B-CT performed in our study. Moreover, based on preliminary studies, all examinations were performed with a tube current of 25 mA with the aim to keep radiation dose at similar level to screening mammography.[15,16] For image reconstructions, a Feldkamp-type filtered back-projection algorithm was used by the nu:view reconstruction software. A smooth kernel $(300\ \mu m^3)$ voxel size and 4 × 4 detector binning were used for ST image reconstruction. A Shepp-Logan kernel of $(150\ \mu m)^3$ voxel size with 2 × 2 detector binning was used for high-resolution (HR) image reconstruction applied for detection and characterization of microcalcifications.

Image Evaluations

Raw image data were reconstructed to 0.3-mm axial slices for ST evaluation (ST reconstruction, ST) and to 0.15-mm axial slices for evaluation of microcalcifications (HR reconstruction, HR). Image analysis was performed on a PACS workstation equipped with a dedicated breast imaging display software (AGFA Impax 6, Mortsel, Belgium) and the possibility to obtain additional sagittal and coronal reformations as well as maximum intensity projection (MIP) reformations with a slice thickness of up to 50 mm.

Subjective Image Quality and Imaging Findings Detection

Subjective image quality evaluation was independently performed by 2 radiologists with 7 years of experience in breast imaging (N.B., M.M.). Each reader in one reading session evaluated all cases. Reformations in the sagittal and coronal plane and corresponding MIP images were initially rated, taking into account the criteria normally applied to mammography according to the PGMI (perfect, good, moderate, inadequate) evaluation system.[21] Accordingly, the following criteria for image quality assessment were applied: (*a*) complete inclusion of the breast tissue (including complete inclusion of the glandular tissue, Chassaignac bursa, and most superficial part of the pectoralis major muscle); (*b*) presence/

absence of subject-related motion artifacts; (*c*) presence/absence of system-related artifacts (eg, "ring" artifact; beam-hardening artifact); and (*d*) symmetrical representation of the 2 breasts, as evaluated in the MIP images in sagittal and coronal reformations, mimicking the mediolateral oblique and craniocaudal mammographic view, respectively. In presence of artifacts, the readers had to indicate whether these were interfering with image interpretation.

The visibility and demarcation of the following breast structures were evaluated in ST and HR as well as in mammography according to a 5-point Likert scale (1 and 5 corresponding to the lowest and highest visibility and demarcation, respectively): skin-air boundary, glandular tissue, fat tissue, and Cooper ligaments.

Moreover, each reader recorded B-CT imaging findings by reporting category (mass, calcification, architectural distortion) and location (side and quadrant) of the lesion. The final reports issued in consensus during the first B-CT dataset evaluation together with the sonographic assessment in case of dense breast or any B-CT finding were used as reference standard.

Objective Image Quality

For each examination, objective image quality measurements were performed in consensus by the 2 readers. Calcifications were measured in mammography and in ST and HR reconstructions as surrogate for the assessment of spatial resolution. For signal and contrast evaluation, an arbitrary defined, circular 1.3 × 1.3 cm region of interest (ROI) was placed in the glandular tissue, in fat tissue, and in the background air. To measure the signal-to-noise ratio (SNR) of the glandular and fat component of the breast, the average attenuation value separately measured in the tissue components (S_{gl} and S_{fat}, respectively) was divided by the standard deviation in the background (SD_{air}) for both reconstruction methods. Signal values were referenced to measurements in air (defined as zero signal). The contrast-to-noise ratio (CNR) was evaluated as the difference between S_{gl} and S_{fat} divided by SD_{air}. The ROIs were copied manually to the same location in ST and HR reconstructions.

Dose Estimation

The radiation dose was evaluated by Monte Carlo (MC) simulations using a commercially available tool (ImpactMC; AB-CT GmbH, Erlangen, Germany). At the first step, the MC tool was validated against the measurements using a standard CT dose index (CTDI) phantom with a diameter of 16 cm and a 10-cm long ionization chamber. The phantom was placed at the isocenter of the breast CT scanner, and the dose values were measured at the central and peripheral positions of the phantom using the protocols summarized in Table 2. In addition, CTDI values free in air were measured for further conversion of the simulated results to absolute dose values. The weighted CTDI ($CTDI_w$) was calculated as follows:

$$CTDI_w = \frac{1}{3} CTDI_c + \frac{2}{3} CTDI_p,$$

where $CTDI_c$ and $CTDI_p$ are the dose integrals measured by the ionization chamber at the center and at the peripheral positions of the 16-cm CTDI phantom, respectively. Then, measured values were compared with the simulated ones, and the relative difference between simulated $CTDI_w$ and measured $CTDI_w$ was defined as follows:

$$\Delta CTDI = \frac{CTDI_w^{simu} - CTDI_w^{meas}}{CTDI_w^{meas}}.$$

After the validation procedure, the MC simulations were performed in cylindrical phantoms of various diameters, starting from 80 mm up to 200 mm, in a step of 20 mm. The material composition was defined as a mixture of 80% and 20% of adipose and glandular tissue, respectively. The kVp and mAs settings for the MC simulations were selected to be equal to those used for the patients' image acquisitions. Simulations were performed using a graphics processing unit cluster with the number of simulated histories set to 2×10^9 to ensure statistically acceptable levels of uncertainty (<1%). The average dose absorbed by each cylinder was calculated based on the 3-dimensional dose distribution obtained from the MC simulations. Then, the patient-specific breast diameter was measured using the B-CT datasets in the middle of the acquired volume, and the radiation dose absorbed by the patient's breast was determined based on MC simulations on the cylindrical phantom with the corresponding diameter.

TABLE 2. Summary of the B-CT Protocol Parameters Used for the MC Code Validation

Parameter	Value
Tube voltage, kVp	60
Tube current, mA	5, 50, 125

B-CT indicates breast computed tomography; MC, Monte Carlo; kVp, kilovoltage peak.

Comfort Assessment

After the B-CT examination, all women were asked to report about their experience during the scan and in particular to rate the comfort of the position and their overall comfort level during the examination on a scale from 1 to 5 (with 5 indicating maximal comfort). In women with previous mammography examinations, a comparison in terms of comfort was also requested (higher, equal, or lower).

Statistical Analysis

The Shapiro-Wilk test showed nonnormal distribution of the data. Descriptive data are provided as median and interquartile range (IQR). Cohen κ coefficient was used to evaluate interobserver agreement between the 2 readers who performed the subjective image quality analysis and categorization of B-CT findings. Bland-Altman plots were used to represent the size differences of microcalcifications measured in mammography and with ST and HR B-CT reconstructions. The Wilcoxon signed rank test was used to compare microcalcification measurements performed in mammography and with ST and HR, glandular tissue SNR (SNR_{gl}), fat tissue SNR (SNR_{fat}), and CNR in the ST and HR. The Bonferroni correction was used to correct for multiple comparison, and a 2-sided *P* value of less than 0.017 (0.05/3) was considered statistically significant. Statistical analyses were performed with commercially available software (SPSS, release 22.0; SPSS Inc, Chicago, IL).

RESULTS

Subject Characteristics

Twelve women (median age, 52.5 years; IQR, 48.7–54 years) were included, and all of them underwent bilateral B-CT. Five women had a previous mammography. Mammography and sonographic images from previous examinations were available in 3 cases performed 18, 24, and 36 months before B-CT; in 2 additional cases, previous mammography was not performed in our hospital and images were not available. American College of Radiology breast density categories were as follows: 2 cases A (16.7%), 2 cases B (16.7%), 5 cases C (41.6%), and 3 cases D (25%). All cases C and D underwent additional sonography. In cases ACR A and B, the 2 radiologists evaluating in consensus the images were confident to exclude the presence of any lesion due to the lack of dense tissue components or any additional finding that could have masked subtle lesions.

TABLE 3. Evaluation of the B-CT Examination

	Inclusion of the Right Breast		Inclusion of the Left Breast		Movement Artifact		Artifacts Right Breast		Artifacts Left Breast		Symmetrical Representation		Calcifications Number		Mass/AD	
n	R_1	R_2	R_1	R_2	R_1	R_2	R_1	R_2	R_1	R_2	R_1	R_2	R_1	R_2	R_1	R_2
1	MP	MP	MP	MP	A	A	RA	RA	RA	RA	Yes	Yes	1	1	M	M
2	Yes	Yes	MP	MP	A	A	RA	RA	RA	RA	Yes	Yes	No	No	No	No
3	GlT	GlT	GlT	GlT	A	A	RA	RA	RA	RA	Yes	Yes	No	No	No	No
4	MP	MP	MP	MP	A	A	RA	RA	RA	RA	Yes	Yes	No	No	No	No
5	Yes	Yes	MP	MP	A	A	RA	RA	RA	RA	Yes	Yes	1	1	No	No
6	Yes	Yes	Yes	Yes	A	A	RA	RA	RA	RA	Yes	Yes	1	1	No	No
7	Yes	Yes	Yes	Yes	A	A	RA	RA	RA	RA	Yes	Yes	No	No	No	No
8	MP	MP	MP	MP	A	A	RA	RA	RA	RA	Yes	Yes	No	No	No	No
9	Yes	Yes	Yes	Yes	A	A	RA	RA	RA	RA	Yes	Yes	No	1	No	No
10	Yes	Yes	Yes	Yes	A	A	RA	RA	RA	RA	Yes	Yes	4	3	No	No
11	Yes	Yes	MP	MP	A	A	RA	RA	RA	RA	Yes	Yes	1	1	No	No
12	Yes	Yes	Yes	Yes	A	A	RA	RA	RA	RA	Yes	Yes	3	3	M	M

B-CT indicates breast computed tomography; AD, architectural distortion; R_1, reader 1; R_2, reader 2; MP, pectoralis major muscle not included; GlT, part of the glandular tissue not completed included at level of the axillary tale; A, absent; RA, ring artifact; M, mass.

Image Evaluations

Subjective Image Quality

Results from image quality assessment are reported in Table 3. Cohen κ showed excellent agreement (κ = 1) between the 2 readers for the image quality assessment and artifact identification. In the total of 24 scanned breasts, the pectoralis major muscle was not included in 9 cases (37.5%) and the external glandular component was not bilaterally included in one (8.3%). In the latter case, the external glandular component was also not included in the previous mammographic examination. None of the B-CT cases exhibited movement artifacts. A "ring artifact," consisting of a thin black circular line in consecutive axial images, was constantly present. The ring artifact was more pronounced in HR reconstructions (Fig. 2) compared with ST. In all cases, this artifact had no effect on image interpretation. No beam-hardening artifacts were present.

Scores assigned to visibility and demarcation of breast structures in ST, HR, and mammography are reported in Table 4. Excellent agreement was found (κ = 1) between the 2 readers for all structures in mammography and for all skin-air boundary evaluations but poor to fair agreement for all other investigated features (κ = 0.12–0.53). Nevertheless, a very high score[4,5] was assigned by the 2 readers in all cases to the glandular and fat tissue demarcation and in all but one case (score 3 by both readers in SR and HR reconstruction) to the representation of the fibrous structures constituting the Cooper ligaments. Both readers assigned a score of 3 to 2/3 cases and a score of 4 to 1/3 cases for glandular and fat tissue demarcation and a score of 3 to 3/3 cases for Cooper ligaments.

Breast Imaging Findings

In 1 woman, 2 oval circumscribed masses were identified on B-CT images in one breast (maximum diameter, 15 mm and 11 mm) that corresponded to simple cysts on ABUS (16 mm and 10 mm, respectively; Fig. 3). In the same woman, 3 additional simple cysts were depicted only on ABUS (maximum diameter median, 8 mm; range, 6–12 mm). All these cysts were stable compared with a previous

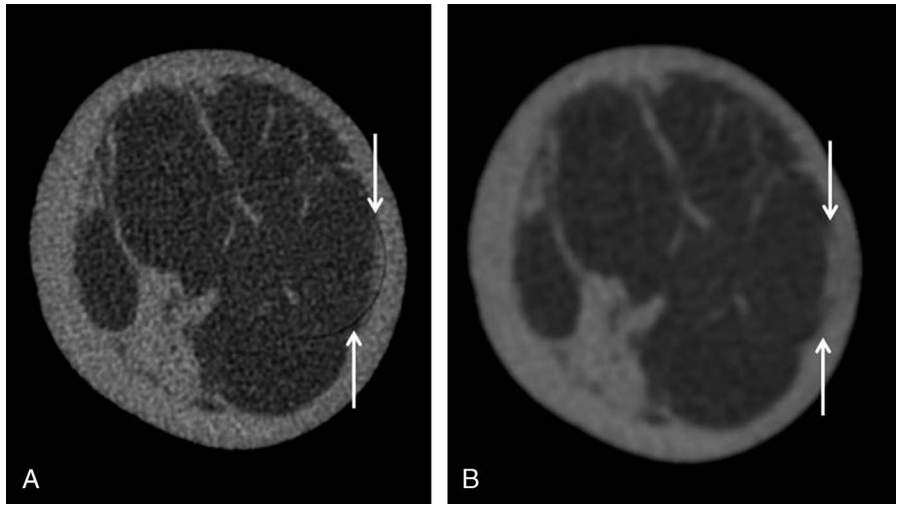

FIGURE 2. Ring artifact in a B-CT image. The artifact is more prominent on HR (A) as opposed to ST (B), however, did not impair image evaluation.

TABLE 4. Visibility and Demarcation of Breast Structures in ST and HR Reconstructions as well as Mammography Evaluated According to a 5-Point Likert Scale (1, Lowest Visibility and Demarcation; 5, Highest Visibility and Demarcation)

	Skin-Air Boundary						Glandular Tissue						Fat Tissue						Cooper Ligaments					
	ST		HR		Mx		ST		HR		Mx		ST		HR		Mx		ST		HR		Mx	
n	R_1	R_2	R_1	R_2	R_1	R_2	R_1	R_2	R_1	R_2	R_1	R_2	R_1	R_2	R_1	R_2	R_1	R_2	R_1	R_2	R_1	R_2	R_1	R_2
1	5	5	5	5	5	5	4	4	4	4	3	3	4	5	4	5	3	3	4	4	4	4	3	3
2	5	5	5	5	NM	NM	4	4	5	5	NM	NM	5	5	4	5	NM	NM	5	4	4	4	NM	NM
3	5	5	5	5	5	5	4	4	5	5	4	4	4	4	4	4	4	4	5	5	4	4	3	3
4	5	5	5	5	NM	NM	4	5	4	5	NM	NM	4	5	4	5	NM	NM	3	3	3	3	NM	NM
5	5	5	5	5	NM	NM	4	5	4	5	NM	NM	4	5	4	5	NM	NM	4	4	4	4	NM	NM
6	5	5	5	5	NM	NM	4	4	4	4	NM	NM	4	4	4	4	NM	NM	4	5	4	5	NM	NM
7	5	5	5	5	NM	NM	5	5	5	5	NM	NM	5	5	4	5	NM	NM	4	4	4	4	NM	NM
8	5	5	5	5	NM	NM	4	4	4	4	NM	NM	4	4	4	4	NM	NM	5	5	4	5	NM	NM
9	5	5	5	5	NM	NM	5	5	5	5	NM	NM	5	5	5	5	NM	NM	4	4	4	4	NM	NM
10	5	5	5	5	5	5	4	5	4	5	3	3	4	5	4	5	4	4	4	4	4	4	3	3
11	5	5	5	5	NM	NM	4	4	4	4	NM	NM	4	4	4	4	NM	NM	4	5	4	5	NM	NM
12	5	5	5	5	NM	NM	4	4	4	4	NM	NM	4	4	4	4	NM	NM	4	4	4	4	NM	NM
	1		1		1		0.44		0.53		1		0.38		0.12		1		0.52		0.34		1	

ST indicates soft tissue reconstruction; HR, high-resolution reconstruction; R_1, reader 1; R_2, reader 2; Mx, mammography; NM, no mammography available.

sonographic examination and were not visible in previous mammograms. In another woman, an oval circumscribed mass was identified on B-CT images (6 mm), which corresponded on ABUS to a circumscribed benign solid lesion (6 mm). Calcifications were depicted in 7/12 cases (58.3%), which were single and unilateral in 5 cases (5/7, 71.4%) and multiple and/or bilateral in other 4 cases (2/7, 28.6%) for a total of 12 calcifications. In 2 cases, previous mammography was available for comparison and calcifications were classified as stable in both cases. In all cases, calcifications had no suspicious distribution. No cases of architectural distortion were observed.

Both readers identified 11/12 (91.7%) calcifications and 3/3 (100%) masses on B-CT images and Cohen κ showed moderate ($\kappa = 0.73$) and excellent ($\kappa = 1$) agreement, respectively. Among the women undergoing additional hand-held ultrasound, in one case, a simple cystic lesion (4 mm) and a circumscribed solid lesion (10 mm) were additionally depicted. Similarly, in another case, a simple cyst (3 mm) and a circumscribed solid lesion (6 mm) were additionally found.

Objective Image Quality

Among the total of 12 calcifications comparison with previous mammograms was possible for 5 calcifications (Figs. 4, 5). Median calcification size on mammography, HR, and ST was 0.6 mm (IQR, 0.5–0.9 mm), 1.1 mm (IQR, 0.7–1.7 mm), and 1.4 mm (IQR, 1.1–1.8 mm), respectively, with significant difference between the measurements performed on HR and ST images ($P = 0.006$) but not between mammography versus HR and ST ($P = 0.102$ and $P = 0.042$, respectively). The Bland-Altman plots referring to the calcification size differences measured in mammography, ST, and HR reconstructions are shown in Figure 6.

Signal-to-noise ratio and CNR values in ST and HR reconstructions are reported in Table 5. In 2 women with an ACR density of A, glandular tissue representation was insufficient to perform ROI measurements, and SNR_{gl} and CNR were not evaluated. Median SNR_{gl}, SNR_{fat}, and CNR were significantly higher in ST than in HR reconstructions ($P < 0.0001$).

Dose Estimation

The differences between measured and simulated CTDIw values (ΔCTDI) are shown in Table 6. The maximum deviation of the simulated to the measured dose was 4.4% at 50 mA, whereas the average absolute difference between measurements and simulations was within 3.6%. The mean dose obtained from MC simulations was 5.08 mGy (range, 4.4–5.7 mGy).

Comfort Assessment

All women included in the study were in a good physical condition (ie, no reported mobility restrictions in daily activity) and could get on and off the examination table without assistance. Position comfort was rated 3 in 2 cases (16.7%), 4 in 9 cases (75%), and 5 in 1 case (8.3%), and overall comfort was rated in 10 cases, 4 (83.3%), and in 2 cases, 5 (16.7%). All women with a previous mammographic examination reported a higher comfort for B-CT, attributed to the absence of breast compression in B-CT. The only complaints concerned a mild discomfort due to the position of the rib cage resting on the table at the margin of the gantry reported by 2 women (16.7%).

DISCUSSION

This study presents the first data obtained from the clinical in vivo application of a new dedicated spiral-B-CT using a photon-counting detector. Breast computed tomography is a cross-sectional imaging technique with a proven higher diagnostic accuracy compared with mammography regarding breast lesions.[11–13] The higher accuracy results from the largely resolved overlapping of the breast tissue and the possibility to analyze imaging findings in multiple anatomical planes from a single scan. Up to now, resolution of B-CT did not reach high enough resolution to visualize microcalcifications, which the new dedicated B-CT can provide. A previous experimental study has been conducted using the same system and included the evaluation of surgical specimens. In this previous study, it has been demonstrated that the system can achieve a spatial isotropic resolution of better than 5 line pairs/mm corresponding to better than 100 μm resolution, with low noise level and under the maximal permitted level of dose exposition.[15] The high resolution, but also the possibility to evaluate the images in different planes, increases and facilitates the characterization of lesions regarding suspicious features such as conspicuity, calcifications, and asymmetries, as well as masses.[14,22,23]

Due to the retrospective nature of our study, no mammography was performed in addition to B-CT, and previous mammography was available only in a limited number of cases, thus precluding a systematic

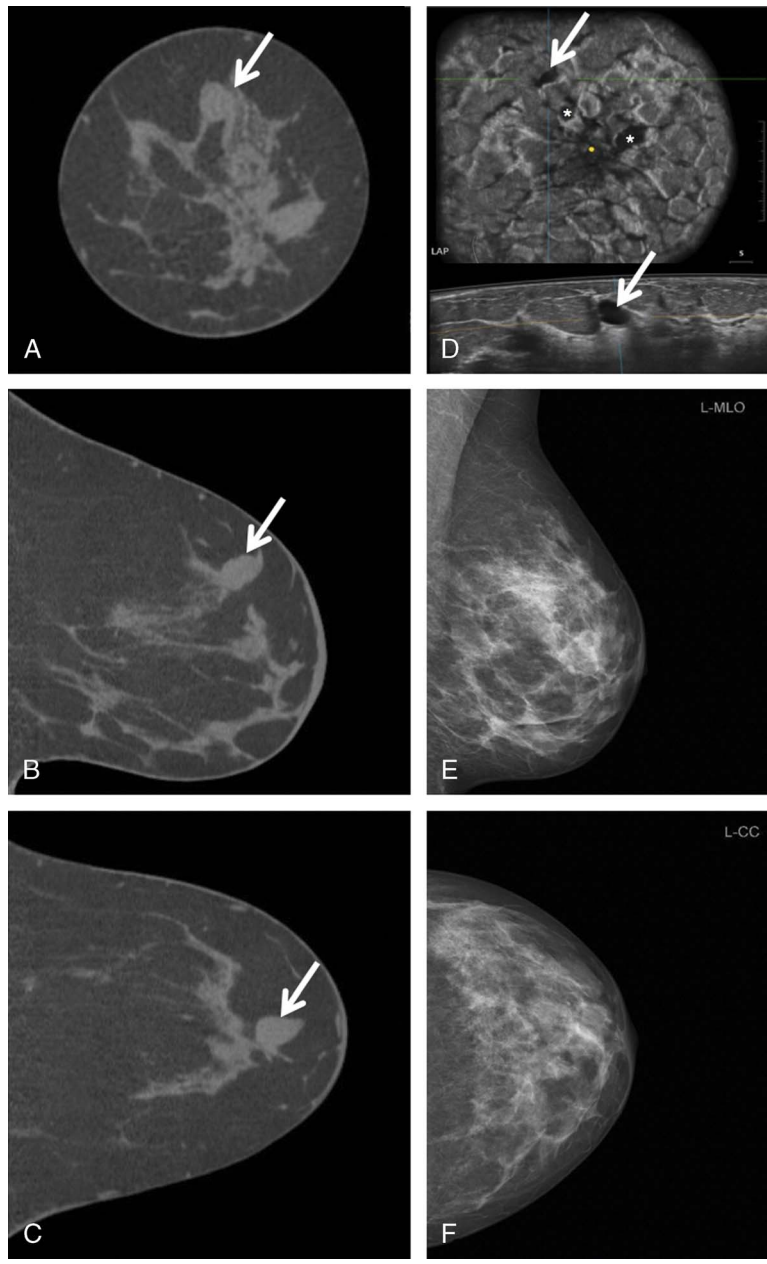

FIGURE 3. Oval circumscribed lesion at 11 to 12 o'clock in the left breast of a 51-year-old woman. The lesion can be easily depicted in the coronal, sagittal, and axial B-CT ST (A–C). The corresponding lesion in coronal and axial ABUS images (D) was a cyst with a maximum diameter of 11 mm that was stable compared with a previous sonographic examination performed 18 months before B-CT. Two additional cysts can be recognized in the coronal ABUS image at 11 and 2 o'clock closer to the nipple (marked with asterisk). Although we consider that some breast density changes could be occurred in the time interval, in mammography (E and F) performed 18 months before B-CT, the cyst was not clearly identifiable.

comparison. Nevertheless, our initial data demonstrate a high B-CT performance in terms of image quality. Visibility and demarcation of breast structures were in general excellent in B-CT with a slightly better performance of the ST reconstruction compared with HR, which is supported by the higher SNR and CNR values. On the other hand, HR outperformed ST reconstruction for determining calcification sizes, with values being similar to those from mammography. Discrepancy in size measurements of calcifications in different reconstruction algorithms in CT is known due to blooming artifacts.[24] In our study, the smallest identified calcification in B-CT as well as in mammography was 0.4 mm. There were no smaller calcifications in B-CT or the available mammograms to verify the size limit of the detection of even smaller calcifications. Further studies are necessary to perform an accurate comparison of calcification size in B-CT and mammography to demonstrate also in vivo that calcification down to 0.1 to 0.2 mm can be identified similar to mammography. Indeed, digital mammography has a spatial resolution of 5 to 9.3 line pairs/mm, whereas previous studies investigating the use of cone beam B-CT have shown that a maximum of 2.6 line pairs/mm can be achieved, ensuring depiction of calcifications down to 0.2 to 0.3 mm.[14,25] In B-CT, higher-contrast resolution can be

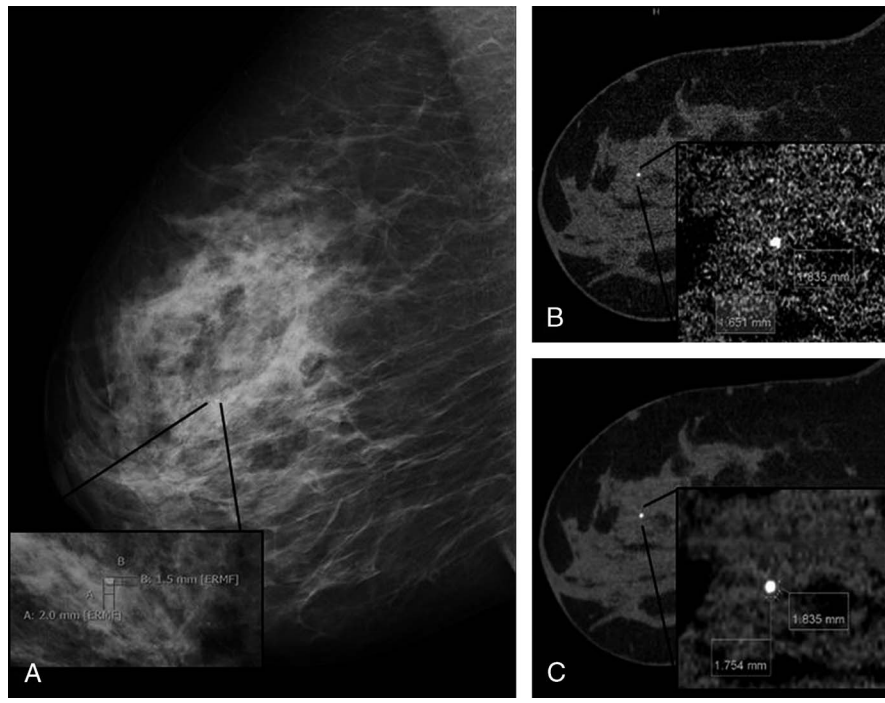

FIGURE 4. A 57-year-old woman with known microcalcification and macrocalcification of the breast. A macrocalcification is visible in the mediolateral oblique mammogram in the central retroareolar region and magnification is provided (A). Mammography was performed 24 months before B-CT. HR (B) and ST (C) and corresponding magnification of the macrocalcification are provided. Although the 2 examinations were performed in a long time interval and variation of calcification size cannot be excluded, similar values of maximal diameter were measured. Concerning B-CT images, almost identical values could be measured in the images obtained with both HR and ST.

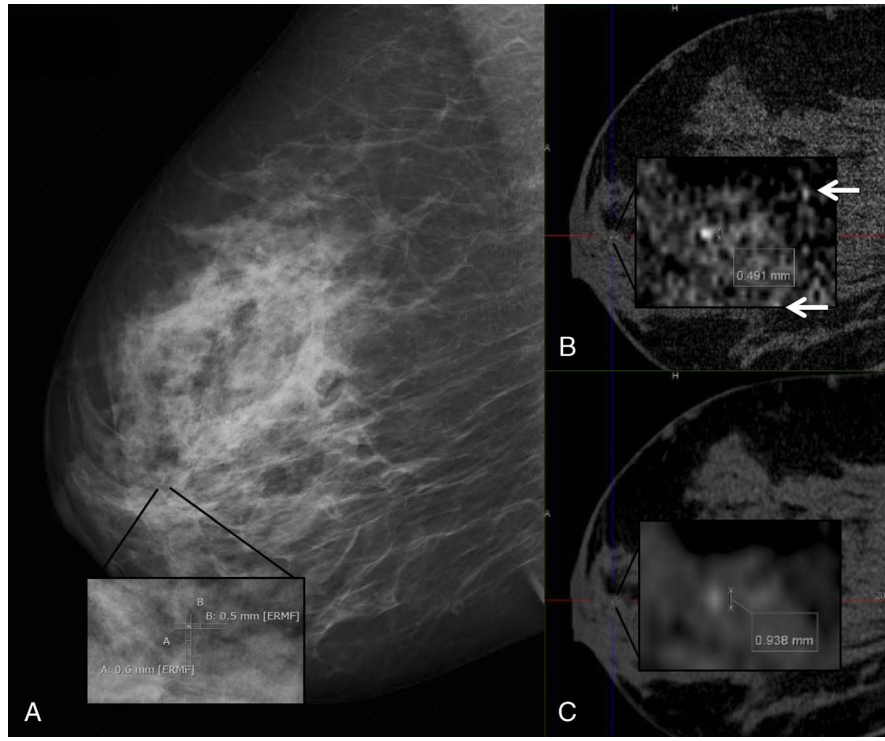

FIGURE 5. Same woman as in Figure 2. A microcalcification is visible in the mediolateral oblique mammogram in the retroareolar region and magnification is provided (A). Mammography was performed 24 months before B-CT. HR (B) and ST (C) and corresponding magnification of the microcalcification are provided. In HR magnification, additional microcalcifications can be recognized (white arrows). Although the 2 examinations were performed in a long time-interval and variation of calcification size could have occurred, similar values of minimum diameter were measured in mammogram and HR. In ST, the minimum diameter was 0.3 mm larger than in HR.

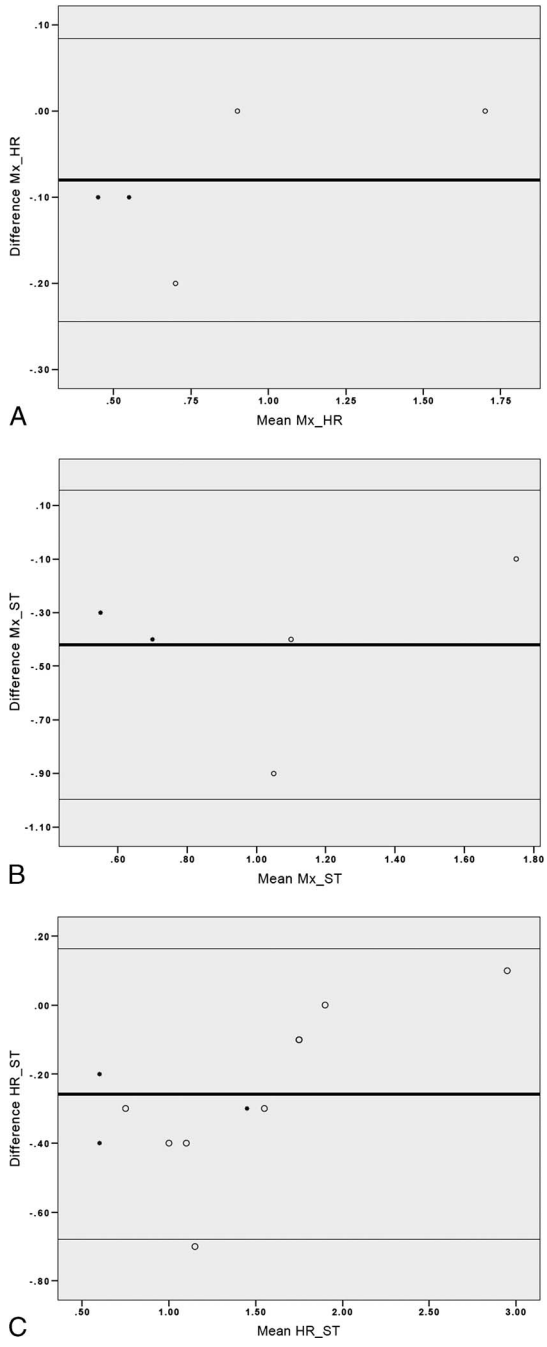

FIGURE 6. Bland-Altman plot comparing calcification measurements performed on mammography versus HR (A), mammography versus ST (B), and HR versus ST (C). The horizontal lines represent the mean and 95% confidence intervals. Black dots represent calcifications smaller than 0.5 mm as measured on at least one among mammography, HR and ST images.

exploited to compensate for the lower spatial resolution. A reasonable approach could combine the evaluation of ST reconstructed images, with their higher CNR to facilitate calcification depiction, followed by a more accurate characterization of calcifications on HR images.

The possibility to obtain sagittal and axial reconstructions as well as MIP reconstructions, simulating MLO and CC projection, respectively, can facilitate and fasten image interpretation. Depiction of the most superficial part of the pectoralis major muscle is desirable as a quality criterion in B-CT scans. Sporadic lack of the pectoralis muscle in the initial CT scans was optimized by improved patient positioning on the scanner table. In only one case, parts of the glandular tissue at axillary tail level were not included in the acquired volume. In this case, the same was also observed in the previous mammography. Nevertheless, the positioning of the patient has to be carefully done by the technician to obtain the optimal coverage and to include as much external glandular component as possible. Limited coverage of axilla and axillary tail compared with mammography is a known limitation of B-CT.[14,26] However, enlarged lymph nodes on otherwise normal mammograms are rarely malignant and clinically significant, and their noninclusion in B-CT images can be considered of negligible clinical value. A comprehensive evaluation of the breast glandular tissue needs to be guaranteed also in women with glandular extension in the axillary tail area by integrating B-CT images with a sonographic evaluation.[27,28] Moreover, additional sonography remains crucial in all women with dense breasts.[13] Indeed, among our records, additional cystic lesions up to 10 mm, completely surrounded by glandular tissue, were not visible in B-CT images an only depicted in sonography due to a lack of a "mass-effect." Due to the presence of a single solid lesion in our series, we could not investigate the diagnostic performance of B-CT for solid versus cystic lesions and also this aspect will be better explored in upcoming studies.

Although we are aware that the high efficacy of screening with mammography on reducing breast cancer mortality relies on the use of standardized protocols with proved high safety and reproducibility and that the implementation of a B-CT in this setting would require an extensive evaluation in a prospective clinical trial, an important immediate advantage of B-CT is that women who previously avoided screening examinations or diagnostic mammograms due to painful compression of their breast can now be motivated to be examined.[29–31] Moreover, due to the advantage of a cross-sectional imaging technique, more information is provided within one single examination, avoiding for example further examinations such as an additional tomosynthesis after an inconclusive mammography. Similar to other studies[12,14,23] having the limitation that all included women were in good physical condition, no significant discomfort during B-CT was reported.

The possibility to apply contrast media on B-CT represents another potential advantage, and this could be an alternative to breast MR imaging in patients otherwise not eligible because of hypersensitivity to contrast media, claustrophobia, or other contraindications to breast MR imaging.[22,32,33]

Usually, in cone-beam B-CT, 2 orthogonal low-dose scout images are initially acquired to set the optimal tube current and achieve the best compromise between dose and contrast-to-noise ratio (CNR).[14] Due to the design of the spiral B-CT acquisition, a scout image is not available and scan parameters need to be defined before data acquisition. In our study, we used a constant tube current of 25 mA and tube voltage of 60 kV across all examinations, resulting in a dose comparable to a conventional screening mammography.[15,16] A homogeneous dose distribution in the breast is a known additional advantage of B-CT compared with mammography.[11] Moreover, the photo-counting technology should allow a further dose reduction due to the higher efficiency of x-ray photon energy conversion into electric charge.[16] Nevertheless, to obtain adequate image quality at the lowest possible dose, further studies are mandatory to investigate the optimal tube current and tube voltage levels depending on the respective clinical indication, breast size, and breast composition. Such investigations may potentially be performed in patients with a high likelihood of radiation therapy or mastectomy (BIRADS 5 and 6 lesions).

The "ring artifact" is a known artifact in CT imaging typically due to malfunction or miscalibration of one or more detectors.[34] Although considering the small number of cases included, that limits definitive conclusions, in our study, similar to a previous study by O'Connell et al,[14] the presence of this artifact did not interfere with

TABLE 5. SNR and CNR for ST and HR Reconstructions

	ST			HR		
	SNR_{gl}	SNR_{fat}	CNR	SNR_{gl}	SNR_{fat}	CNR
Median	147.8	115.7	33.0	47.5	36.9	10.5
IQR	141.5–153.9	108.6–122.2	27.2–34.7	45.0–48.6	35.6–37.8	8.8–11.0
Minimum	119.1	97.1	20.7	41.2	31.3	5.9
Maximum	169.9	133.3	38.1	57.9	43.9	14.0

SNR indicates signal-to-noise ratio; CNR, contrast-to-noise ratio; ST, soft tissue reconstruction; HR, high-resolution reconstruction; IQR, interquartile range; SNR_{gl}, SNR glandular tissue; SNR_{fat}, SNR fat tissue.

image interpretation. Even considering the possibility that a singular microcalcification could be shadowed by the artifact, it would not have any clinical consequence. Moreover, the artifact appearance does not reproduce any known microcalcification distribution pattern, thus minimizing the possibility to miss clinically significant microcalcifications even in case that one of them is shadowed by the artifact. In addition, we found no motion artifacts in our image data sets. None of the women presented a breast tissue marker to allow for comparison in terms of beam-hardening artifacts. A previous phantom study showed a significant effect of breast markers on image quality, and this factor should be considered when women with previous breast interventions undergo B-CT.[35]

As the images are cross-sectional and can be evaluated using different planes, a longer reading time compared with mammograms is foreseeable. Nevertheless, optimization of image reconstruction has the potential to assist the radiologist for the depiction and characterization of breast lesions to expedite the reading process.

Our study has several limitations including the small number of retrospective cases and, as mentioned preciously, the lack of a parallel mammography for direct comparison. In the few cases with availability of a previous mammography, the mammography was performed a rather long time before the B-CT, thus limiting a rigorous comparison. Also, none of the patients had a malignant lesion. Nevertheless, our work aimed at a presentation of the first in vivo images obtained with a new approved and commercially available B-CT system and to show its diagnostic potential. In addition, related to the lack of parallel mammography, the lack of comparison in dose estimation between mammography and B-CT has to be addressed. A systematic comparison of dose estimation as well as diagnostic accuracy for the 2 imaging modalities will be the goal of upcoming prospective studies.

In conclusion, the new dedicated spiral B-CT equipped with a photon-counting detector provides high-quality images at low radiation dose and shows considerable potential for screening and diagnosis of breast cancer, along with improved patient comfort compared with conventional mammography.

TABLE 6. Weighted CTDI Values Derived from Measurements and Simulations Including the Differences

	CTDIw/mGy		
Method	**5 mA**	**50 mA**	**125 mA**
Measurements	1.03	10.49	16.02
Simulations	1	10.03	25.08
Difference in %	2.9	4.4	3.6

CTDIw indicates weighted CT dose index.

ACKNOWLEDGMENTS

We thank Daniel Kolditz, PhD, for his technical support.

REFERENCES

1. Paap E, Holland R, den Heeten GJ, et al. A remarkable reduction of breast cancer deaths in screened versus unscreened women: a case-referent study. *Cancer Causes Control*. 2010;21:1569–1573.
2. Tabar L, Vitak B, Chen THH, et al. Swedish two-county trial: impact of mammographic screening on breast cancer mortality during 3 decades. *Radiology*. 2011; 260:658–663.
3. Tabar L, Yen MF, Vitak B, et al. Mammography service screening and mortality in breast cancer patients: 20-year follow-up before and after introduction of screening. *Lancet*. 2003;361:1405–1410.
4. Kolb TM, Lichy J, Newhouse JH. Comparison of the performance of screening mammography, physical examination, and breast US and evaluation of factors that influence them: an analysis of 27,825 patient evaluations. *Radiology*. 2002;225: 165–175.
5. Ciatto S, Houssami N, Bernardi D, et al. Integration of 3D digital mammography with tomosynthesis for population breast-cancer screening (STORM): a prospective comparison study. *Lancet Oncol*. 2013;14:583–589.
6. Friedewald SM, Rafferty EA, Rose SL, et al. Breast cancer screening using tomosynthesis in combination with digital mammography. *JAMA*. 2014;311: 2499–2507.
7. Rafferty EA, Durand MA, Conant EF, et al. Breast cancer screening using tomosynthesis and digital mammography in dense and nondense breasts. *JAMA*. 2016;315:1784–1786.
8. Skaane P, Bandos AI, Gullien R, et al. Comparison of digital mammography alone and digital mammography plus tomosynthesis in a population-based screening program. *Radiology*. 2013;267:47–56.
9. Clauser P, Baltzer PAT, Kapetas P, et al. Synthetic 2-dimensional mammography can replace digital mammography as an adjunct to wide-angle digital breast tomosynthesis. *Invest Radiol*. 2019;54:83–88.
10. Maldera A, De Marco P, Colombo PE, et al. Digital breast tomosynthesis: dose and image quality assessment. *Phys Med*. 2017;33:56–67.
11. Boone JM, Nelson TR, Lindfors KK, et al. Dedicated breast CT: radiation dose and image quality evaluation. *Radiology*. 2001;221:657–667.
12. Lindfors KK, Boone JM, Nelson TR, et al. Dedicated breast CT: initial clinical experience. *Radiology*. 2008;246:725–733.
13. Wienbeck S, Uhlig J, Luftner-Nagel S, et al. The role of cone-beam breast-CT for breast cancer detection relative to breast density. *Eur Radiol*. 2017;27:5185–5195.
14. O'Connell A, Conover DL, Zhang Y, et al. Cone-beam CT for breast imaging: radiation dose, breast coverage, and image quality. *Am J Roentgenol*. 2010;195: 496–509.
15. Kalender WA, Kolditz D, Steiding C, et al. Technical feasibility proof for high-resolution low-dose photon-counting CT of the breast. *Eur Radiol*. 2017;27:1081–1086.
16. Kalender WA, Beister M, Boone JM, et al. High-resolution spiral CT of the breast at very low dose: concept and feasibility considerations. *Eur Radiol*. 2012;22:1–8.
17. von Spiczak J, Mannil M, Peters B, et al. Photon counting computed tomography with dedicated sharp convolution Kernels tapping the potential of a new technology for stent imaging. *Invest Radiol*. 2018;53:486–494.
18. Leng S, Rajendran K, Gong H, et al. 150-μm spatial resolution using photon-counting detector computed tomography technology: technical performance and first patient images. *Invest Radiol*. 2018;53:655–662.

19. Miller D, Livingstone V, Herbison P. Interventions for relieving the pain and discomfort of screening mammography. *Cochrane Database Syst Rev.* 2008;CD002942.
20. Sickles EA, D'Orsi CJ, Bassett LW, et al. *ACR BI-RADS Mammography. ACR BI-RADS Atlas, Breast Imaging Reporting and Data System*. Reston, VA: American College of Radiology; 2013.
21. Programme NHSBS. *Quality assurance guidelines for radiographers 30, NHS Breast screening programme*. 1994.
22. Wienbeck S, Fischer U, Luftner-Nagel S, et al. Contrast-enhanced cone-beam breast-CT (CBBCT): clinical performance compared to mammography and MRI. *Eur Radiol*. 2018;28:3731–3741.
23. He N, Wu YP, Kong Y, et al. The utility of breast cone-beam computed tomography, ultrasound, and digital mammography for detecting malignant breast tumors: a prospective study with 212 patients. *Eur J Radiol*. 2016;85:392–403.
24. Gutjahr R, Halaweish AF, Yu ZC, et al. Human imaging with photon counting-based computed tomography at clinical dose levels: contrast-to-noise ratio and cadaver studies. *Invest Radiol*. 2016;51:421–429.
25. Lazzari B, Belli G, Gori C, et al. Physical characteristics of five clinical systems for digital mammography. *Med Phys*. 2007;34:2730–2743.
26. Wienbeck S, Lotz J, Fischer U. Review of clinical studies and first clinical experiences with a commercially available cone-beam breast CT in Europe. *Clin Imaging*. 2017;42:50–59.
27. Lee CH, Giurescu ME, Philpotts LE, et al. Clinical importance of unilaterally enlarging lymph nodes on otherwise normal mammograms. *Radiology*. 1997;203:329–334.
28. Lee SH, Yi A, Jang MJ, et al. Supplemental screening breast US in women with negative mammographic findings: effect of routine axillary scanning. *Radiology*. 2018;286:830–837.
29. Gøtzsche PC, Nielsen M. Screening for breast cancer with mammography. *Cochrane Database Syst Rev*. 2011;CD001877.
30. Nystrom L, Andersson I, Bjurstam N, et al. Long-term effects of mammography screening: updated overview of the Swedish randomised trials. *Lancet*. 2002;359:909–919.
31. Independent UK Panel on Breast Cancer Screening. The benefits and harms of breast cancer screening: an independent review. *Lancet*. 2012;380:1778–1786.
32. Uhlig J, Fischer U, Surov A, et al. Contrast-enhanced cone-beam breast-CT: analysis of optimal acquisition time for discrimination of breast lesion malignancy. *Eur J Radiol*. 2018;99:9–16.
33. Huckle JE, Altun E, Jay M, et al. Gadolinium deposition in humans when did we learn that gadolinium was deposited in vivo? *Invest Radiol*. 2016;51:236–240.
34. Barrett JF, Keat N. Artifacts in CT: recognition and avoidance. *Radiographics*. 2004;24:1679–1691.
35. Wienbeck S, Nowak C, Zapf A, et al. Artifacts caused by breast tissue markers in a dedicated cone-beam breast CT in comparison to full-field digital mammography. *Acad Radiol*. 2017;24:908–915.